JACS Au
AN OPEN ACCESS JOURNAL OF THE AMERICAN CHEMICAL SOCIETY

pubs.acs.org/jacsau
Article

Subsurface Hydride Formation Leads to Slow Surface Adsorption Processes on a Pd(111) Single-Crystal Electrode in Acidic Electrolytes

Xiaoting Chen, Kasinath Ojha, and Marc T. M. Koper*

Cite This: *JACS Au* 2023, 3, 2780−2789
Read Online

ABSTRACT: Palladium is one of the most important catalysts due to its widespread use in heterogeneous catalysis and electrochemistry. However, an understanding of the electrochemical processes and interfacial phenomena at Pd single-crystal electrodes/electrolytes is still scarce. In this work, the electrochemical behavior of the Pd(111) electrode was studied by the combination of cyclic voltammetry (CV) and electrochemical impedance spectroscopy (EIS) in different acidic electrolytes, namely, sulfuric acid, perchlorate acid, methane sulfonic acid, and hydrofluoric acid. An analysis of CV profiles shows the strong adsorption of all anions at low electrode potential, partially overlapping with underpotential deposited hydrogen (UPD-H), leading to the appearance of a pair of sharp peaks in what would be considered the "hydrogen region". All anions studied (HSO_4^-, ClO_4^-, $CH_3SO_3^-$, and F^-) adsorb specifically and interact with (or effectively block) the surface-adsorbed hydroxyl phase formed on the Pd(111) terrace at higher potentials. Strikingly, the scan rate-dependent results show that the process of anion adsorption and desorption is a kinetically rather slow step. EIS measurements show that the exact mechanism of this slow anion ad/desorption process actually stems from (sub)surface phenomena: the direct hydrogen insertion into Pd lattice (hydrogen subsurface absorption) commences from ca. 0.40 V and leads to the formation of (subsurface) Pd hydrides (PdH_x). We argue that the subsurface hydrogen phase significantly alters the work function and thereby the kinetics of the anion adsorption and desorption processes, leading to irreversible peaks in the voltammetry. This precise understanding is important in guiding further fundamental work on Pd single crystals and will be crucial to advancing the eventual design of optimized Pd electrocatalysts.

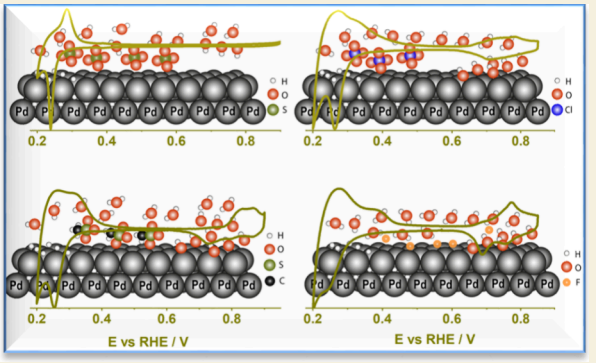

KEYWORDS: *Pd(111) single crystal electrode, cyclic voltammetry, electrochemical impedance spectroscopy, anion adsorption, palladium hydrides*

INTRODUCTION

Palladium metal can absorb a large quantity of hydrogen (i.e., accommodate hydrogen atoms into palladium lattice), which is important in hydrogen storage, metal-hydride batteries, and hydrogen purification. The palladium−hydrogen system has been extensively studied in the gas phase for more than one century. Palladium electrodes are of increasing interest because of their excellent performance for sustainable energy storage and conversion reactions, including electrochemical formic acid/methanol oxidation,[1−3] electrocatalytic reduction of glyceraldehyde, dihydroxyacetone,[4] acetol,[5] and acetophenone,[6] and the electrocatalytic hydrogenation of organic molecules in general. The electrochemical reduction of carbon dioxide on a Pd electrode has been extensively studied recently since Pd electrocatalysts exhibit high selectivity toward formic acid/formate production at low overpotentials.[7−10] Palladium also has good activity for reducing nitrite into less harmful nitrogen gas and useful ammonia products,[11,12] which are of interest for minimizing nitrogen-related pollution and closing the nitrogen cycle. Despite the significant qualitative evidence for the enhanced activity of Pd surfaces for various electrochemical reactions, a more quantitative understanding of the specific electrochemical properties of palladium has been less forthcoming.

The electrochemistry of Pt-group single-crystal electrodes, especially Pt,[13,14] Ir,[15,16] Rh,[17] and Ru,[18,19] is relatively mature and expansive, especially regarding the relation between structure, (adsorption) activity, and selectivity of electrocatalytic reactions. However, studies devoted to single-crystal electrodes of Pd are more scarce, which arise partially from the

Received: June 28, 2023
Revised: September 5, 2023
Accepted: September 8, 2023
Published: September 27, 2023

https://doi.org/10.1021/jacsau.3c00343
JACS Au 2023, 3, 2780−2789

difficulty of preparing Pd single crystals as well as from the effect that palladium absorbs substantial amounts of hydrogen below 0.2 V, masking other reactions taking place on its surface. Therefore, over the past decades, pseudomorphically grown palladium overlayers have been used as an alternative for well-ordered Pd single-crystal electrodes.[20] For instance, Gabrielli et al. performed systematic investigations of hydrogen adsorption/absorption in palladium films obtained by electrodeposition, from a few monolayers (ML) up to several micrometers.[21] One of their main results was that the cyclic voltammogram of very thin Pd films grown epitaxially on Au(111) showed separate hydrogen adsorption and absorption regions, while these processes started at the same potential on bulk Pd (thickness of over 4000 ML, ∼1.6 μm). Generally, palladium hydrides form two phases, α- and β-PdH, with a distinct phase transition,[22,23] and the hydrogen evolution reaction occurs only after β-PdH formation.[24] Characterizing the nature of the anion and cation adsorption at the Pd electrode/electrolyte surface under electrochemical conditions is an aspect of foremost importance for its influence on reaction kinetics, in either a promoted or inhibited fashion.[25] Thus, many studies have also reported the exploration of hydrogen/anion adsorption processes on palladium mono- and multilayers grown epitaxially on Pt basal planes.[26−28] Specifically, our own work has elucidated that the so-called "hydrogen region" on the Pd monolayer on Pt(111) surface is rather a "hydrogen-hydroxyl-cation−anion" region; that is, its exact voltammetric features depend on the interaction with all four species, not only with hydrogen.

To better understand the exact nature of the special reactivity of palladium, detailed investigations on atomically well-defined single-crystal bulk Pd are highly desirable. Electrochemical characterization of Pd single-crystal electrodes started after the introduction of the inductive heating technique.[29,30] Hoshi et al. carried out a considerable amount of work on Pd single-crystal electrodes with low- and high-index planes to explore (bi)sulfate anion adsorption[31,32] and CO[33] adsorption processes by infrared reflection absorption spectroscopy (IRAS). Later, they continued with a series of systematic experiments to describe the cyclic voltammograms of Pd-stepped electrodes.[34−37] All studies specifically focused on the effect of introducing different types of steps with different step densities, on voltammetric peaks in the more positive potential region (0.65 V < E < 1.20 V) related to hydroxide/oxide formation on Pd surfaces. However, cycling to such high potentials always induces irreversibility in the subsequent cycles, suggesting that the formation of O_{ads} is accompanied by a significant restructuring of the Pd surface. On the other hand, research on the underpotential deposition of hydrogen, H_{upd}, and the adsorption of anions on Pt-group single-crystal electrodes provides a "fingerprint" of high-quality single-crystal surfaces under electrochemical conditions. A great deal of knowledge has been gathered about the chemical species responsible for the well-defined and reproducible voltammetric profile of single-crystal Pt-group metal electrodes.[38] However, there are very few detailed studies on the reversible H_{upd} and anion adsorption processes on Pd single-crystal electrodes.[39] These studies often assume that perchlorate electrolytes are nonadsorbing, as for Pt.

It is the objective of this work to propose a detailed understanding of quantitative benchmark voltammograms for the Pd(111) electrode in four common electrolytes, namely, sulfuric acid, perchlorate acid, methanesulfonic acid, and hydrofluoric acid. We focus on the fundamental aspects of H_{upd} and anion ad/desorption processes. Therefore, the limits of the potential sweep are imposed by the onset potential of substantial amounts of hydrogen absorption below 0.20 V and the onset of oxide formation around 1.0 V. We show that all anions exhibit specific adsorption on Pd(111), including fluoride and perchlorate, and further explore the nature of the unexpectedly sluggish kinetics behind the anion adsorption−desorption process on the Pd(111) electrode in the low potential region. Strikingly, we show that the slowness of anion adsorption on Pd(111) is intimately related to the formation of subsurface hydrogen.

RESULTS AND DISCUSSION

Cyclic voltammetry was first conducted in 0.1 M H_2SO_4 at a scan rate of 50 mV s^{-1} to facilitate comparison to reliable literature data.[29,40−42] Figure 1a represents the first cycle

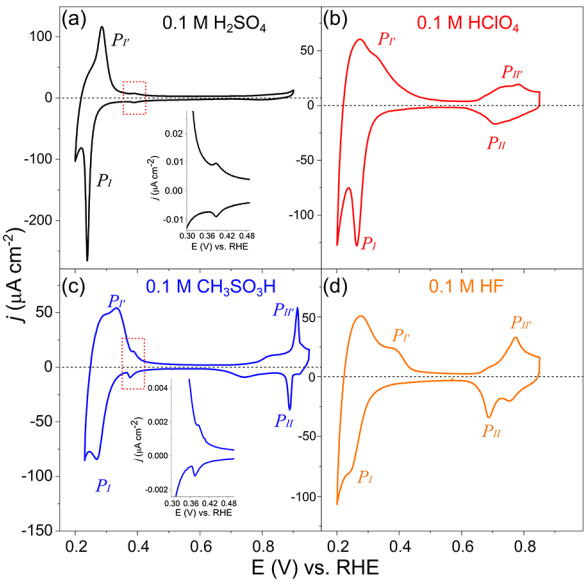

Figure 1. Cyclic voltammograms of Pd(111) electrode recorded in (a) 0.1 M H_2SO_4, (b) 0.1 M $HClO_4$, (c) 0.1 M CH_3SO_3H, and (d) 0.1 M HF solutions. Scan rate: 50 mV s^{-1}. The inset in (a) and (c) represents a magnification of the anion adsorption layer phase transition peak (marked by a red dash square).

recorded after inductive heating of the Pd(111) electrode in an argon atmosphere with immersion at 0.45 V_{RHE} and starting the potential scan in the negative direction. The cyclic voltammogram of Pd(111) in 0.1 M H_2SO_4 (Figure 1a) shows the presence of a pair of sharp peaks (P_I and $P_{I'}$), slightly irreversible, with a peak potential of 0.28 V_{RHE} (PI') in the positive-going scan, and of 0.24 V_{RHE} (P_I) in the negative-going scan. In agreement with the voltammetry of Pd-monolayer modified Pt(111) in 0.1 M H_2SO_4,[28] the sharpness of the peak (P_I and $P_{I'}$) suggests the replacement of adsorbed species, i.e., hydrogen replaced by (bi)sulfate (eq 1) and vice versa. Hoshi et al. have claimed that these redox peaks only occur on Pd surfaces with more than three atomic rows of 111-terrace.[37]

$$H^+ + (y + 1)e^- + y\text{anion}_{ads} \leftrightharpoons H_{ads} + y\ \text{anion}^- \quad (1)$$

https://doi.org/10.1021/jacsau.3c00343
JACS Au 2023, 3, 2780−2789

Following the replacement of (bi)sulfate by hydrogen in the negative-going scan, the hydrogen adsorption (eq 2) and absorption processes (eqs 3 and 4) proceed simultaneously on Pd(111) at potentials below 0.24 V_{RHE}:

$$H_3O^+ + e^- + Pd \leftrightharpoons Pd - H_{ads} + H_2O \quad (2)$$

$$Pd - H_{ads} + Pd(subsurface) \leftrightharpoons Pd(subsurface) - H_{abs} + Pd \quad (3)$$

$$Pd(subsurface) - H_{abs} \leftrightharpoons Pd(bulk) - H_{abs} \quad (4)$$

A further increase in the cathodic current at more negative potentials is due to the hydrogen absorption into the Pd(111) bulk crystal (eq 4) and the voltammogram remains essentially unchanged (as shown in Figure S2), which indicates the ability to reversibly absorb and store hydrogen into the Pd lattice. Accommodating considerable amounts of hydrogen atoms into palladium lattice after applying a critical negative potential (or a number of cycles) may cause irreversible changes in surface morphology; the understanding of this process would require further study also on other Pd single-crystal electrodes besides Pd(111), i.e., Pd(100) and Pd(110). By contrast, the features observed in the first cycle described above change totally when the upper potential limit is extended to the potential where the Pd-oxide formation commences, i.e., 1.0 V_{RHE}, because PdO_X causes the surface roughening of the well-ordered Pd(111) surface.[29,43]

It is noteworthy that the corresponding anodic peak at 0.28 V_{RHE} ($P_{I'}$) is less sharp than the cathodic peak at 0.24 V_{RHE} (P_I), which can be ascribed to irreversibility in the superposition of desorption of absorbed hydrogen (eqs 3 and 4) and the replacement reaction between the adsorbed-hydrogen and (bi)sulfate (eq 1). The inset in Figure 1a shows a pair of reversible peaks at 0.39 V_{RHE}, which arises from a first-order phase transition of the disordered (bi)sulfate adlayer into a $(\sqrt{3} \times \sqrt{7})$ commensurate phase,[41,44] quite similar to the phase transition in (bi)sulfate adlayer on Pt(111) electrodes (peaks at 0.50 V_{RHE}, Figure S1a). Previous electrochemical in situ Fourier Transform Infrared Spectroscopy (FTIRS) studies also found that at the Pd(111)/0.1 M H_2SO_4 interface, there is a single band from the (bi)sulfate adsorbate at ca. 1200 cm^{-1} in the potential range from 0.3 to 0.7 V,[45] similar to that observed on Pt(111)[46] and $Pd_{ML}Pt(111)$[20] electrodes. The specific adsorption of the (bi)sulfate adlayer completely blocks the Pd(111) surface in the more positive potential window between 0.60 and 0.90 V_{RHE}. The result here strongly suggests much stronger anion adsorption on Pd(111) than on Pt(111) because the sulfate adsorption/desorption peak happens at a much less positive potential and overlaps with hydrogen adsorption/desorption, very similar to what has been observed on the $Pd_{ML}Pt(111)$ electrode.[28] The cyclic voltammogram of Pd(111) in 0.1 M H_2SO_4 here (Figure 1a) is identical to those reported previously[29,40−42] which confirms the high quality of the prepared Pd(111) electrode. The anion adsorption process (eq 2) is ascribed specifically to the electrolyte anions (HSO_4^-, ClO_4^-, $CH_3SO_3^-$, and F^-), while OH adsorption is excluded in this low potential window as we will discuss in the following part (Figures 3 and S4).

In perchloric acid, Figure 1b shows the presence of a pair of peaks, slightly irreversible, with a peak potential of 0.31 V_{RHE} ($P_{I'}$) in the positive-going scan and of 0.29 V_{RHE} (P_I) in the negative-going scan. In agreement with the (bi)sulfate adsorption in Figure 1a, the sharp P_I peak suggests the involvement of perchlorate anion desorption rather than a pure hydrogen underpotential region[40] as observed on the Pt(111) electrode, which is again similar to the behavior of perchlorate on the $Pd_{ML}Pt(111)$ electrode (Figure S1b). We will discuss specific perchlorate adsorption in more detail in Figure 2. We

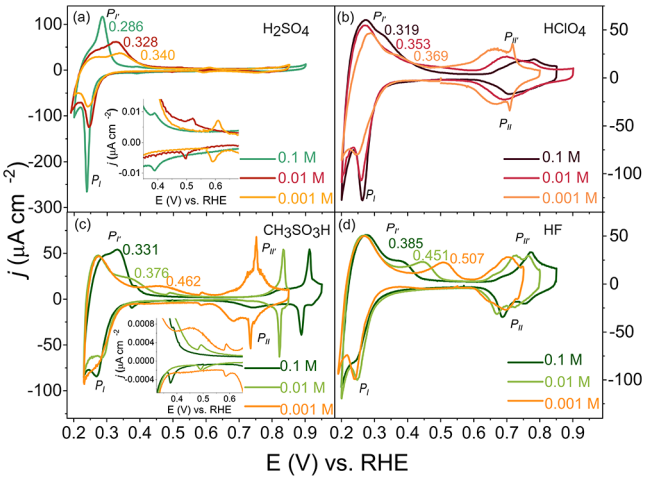

Figure 2. Cyclic voltammograms of Pd(111) electrode in (a) 0.1, 0.01, and 0.001 M H_2SO_4, (b) 0.1, 0.01, and 0.001 M $HClO_4$, (c) 0.1, 0.01, and 0.001 M CH_3SO_3H, and (d) 0.1, 0.01, and 0.001 M HF. Scan rate: 50 mV s^{-1}. The inset in (a) and (c) represents a magnification of the anion adsorption layer phase transition peak.

find that the peaks correlated with the replacement of adsorbed species, i.e., hydrogen and perchlorate, were very sensitive to the quality of the surface, and they are observed only on a well-prepared Pd(111) surface (as shown in Figure S3). For instance, the voltammetric peak of 0.31 V_{RHE} ($P_{I'}$) of Pd(111) in perchloric acid was either not observed[29] or (mis-) interpreted as simply hydrogen underpotential deposition or absorption in previous studies.[40,42] Therefore, particular attention should be paid to the cleanliness and order of the system, as the presence of contaminants and/or an improper inductive heating-annealing procedure greatly influences the Pd single crystal voltammetric profiles and thus their analysis.

Between 0.40 and 0.60 V_{RHE}, there is a very low current in the CV of Pd(111), and this is traditionally called the "double layer region", assuming that the current flowing in this region is due only to capacitive charging of the electric double layer and that there are no adsorbed species. However, note that we do consider that Pd(111) is covered with specifically adsorbed perchlorate in this potential window so that this is the capacitive current of a perchlorate-covered Pd(111) electrode, and there may still be some pseudocapacitive charging current if the perchlorate coverage is changing (though this seems minor). As the potential increases from 0.60 to 0.95 V_{RHE}, there is a broad feature followed by a peak at 0.78 V_{RHE} ($P_{II'}$) (with the corresponding reversible feature in the negative-going scan). This broad feature is interpreted as hydroxyl adsorption:

$$H_2O + Pd \leftrightharpoons Pd - OH_{ads} + e^- + H^+ \quad (5)$$

https://doi.org/10.1021/jacsau.3c00343
JACS Au 2023, 3, 2780−2789

The voltammogram of Pd(111) in 0.1 M CH_3SO_3H in Figure 1c also shows the replacement of adsorbed hydrogen by adsorbed anion, i.e., methanesulfonate, in a pair of peaks, with a peak potential of 0.33 V_{RHE} ($P_{I'}$) in the positive-going scan and of 0.27 V_{RHE} (P_I) in the negative-going scan. A pair of reversible peaks at 0.40 V_{RHE} presumably arises from a phase transition of the adsorbed methanesulfonate adlayer based on a similar observation for the (bi)sulfate adlayer. The "double layer region" (but note again the comment made in the previous paragraph) and "OH_{ads} feature" are observed at 0.40 < E < 0.60 V_{RHE} and 0.60 < E < 0.95 V_{RHE}, respectively. The combination of a broad and a sharp peak of 0.90 V_{RHE} ($P_{II'}$) is very typical for a disorder−order transition in the adsorbate layer, i.e., hydroxyl layer (broad peak at a lower coverage, sharp peak at a higher coverage).[47]

In hydrofluoric acid, Figure 1d shows a pair of rather sharp peaks in the "hydrogen region", which suggests again that the processes underlying these peaks are a replacement reaction of adsorbed hydrogen and adsorbed fluoride, very irreversible, with a peak potential of 0.37 V_{RHE} ($P_{I'}$) in the positive-going scan and of 0.25 V_{RHE} (P_I) in the negative-going scan. The "double layer region" and "OH_{ads} feature" are observed at 0.40 < E < 0.60 V_{RHE} and 0.60 < E < 0.90 V_{RHE}, respectively, similar to perchloric acid.

Based on the combined results in 0.1 M H_2SO_4, 0.1 M $HClO_4$, 0.1 M CH_3SO_3H, and 0.1 M HF solutions, we conclude that the voltammograms of the Pd(111) electrode in acidic electrolytes show three main features: adsorbed hydrogen H_{ads} at the lowest potentials (0.20 < E < 0.45 V_{RHE}), with the replacement of H_{ads} by anion adsorption (with peak potentials of 0.28, 0.31, 0.33, and 0.37 V_{RHE} in the positive-going scan for HSO_4^-, ClO_4^-, $CH_3SO_3H^-$, and F^-, respectively) and an adsorption−desorption peak for OH adsorbed on (111) terraces (0.60 < E < 0.95 V_{RHE}). The order in peak potential for the different anions is a measure of their adsorption strength to the Pd(111) surface, with (bi)sulfate binding being the strongest and fluoride binding the weakest. These results indicate that the electrochemical behavior of the Pd(111) surface in 0.1 M $HClO_4$, 0.1 M CH_3SO_3H, and 0.1 M HF solutions is significantly different from the Pt(111) electrode. On Pt(111), these anions are considered to be nonspecifically adsorbed, and the voltammograms for these different electrolytes are very similar (see the CVs for Pt(111) in ClO_4^-, $CH_3SO_3H^-$, and F^- in Figure S1). The classic "hydrogen region" identified for the pristine Pt(111) surface clearly involves specific anion adsorption for the bulk Pd(111) electrode. For a Pd monolayer decorated Pt(111) surface, it has even been characterized as a 'hydrogen-hydroxyl-anion−cation' region[28] (Figure S1). The high affinity for anion adsorption has been ascribed to the significantly lower work function of Pd compared to Pt.

To further support our interpretation of the Pd(111) CV, we show in Figure 2 the evolution of the blank CV as a function of acid concentration, from pH 1 to 3. The CV is plotted on a reversible hydrogen electrode (RHE) scale so that any features that would be only related to the reversible adsorption/desorption of H or OH should not shift on this potential scale. Regarding the $P_I/P_{I'}$ couple, ascribed to the replacement of adsorbed hydrogen by adsorbed anions (and vice versa), we observe the following. The potential of the anion adsorption, replacing H adsorption, i.e., peak $P_{I'}$, shifts to more positive potentials with decreasing acid concentration, for all anions. The shift is more pronounced for more weakly adsorbed anions, especially fluoride. Since a purely reversible hydrogen adsorption/desorption peak would not shift with pH on the RHE scale, this shift must be due to the involvement of anions. A lower anion concentration leads to a weaker adsorption at a given potential, and hence to higher adsorption peak potential. The potential of zero free charge (E_{pzfc}) of a metal electrode in contact with a solution refers to the potential where the nonfaradaic ("free") excess electronic charge on the electrode equals zero.[48] The anion adsorption may be influenced by pH as the potential of zero free charge (E_{pzfc}) shifts positively on the RHE scale with the increasing pH ($E_{pzfc} = E^\circ_{pzfc} + 0.059$ pH), and therefore, the electrode surface becomes more negatively charged with the increasing pH at the same applied potential on the RHE scale. In the negative-going scan, the P_I peak (at 0.24, 0.29, and 0.27 V_{RHE} for HSO_4^-, ClO_4^-, and $CH_3SO_3H^-$) is observed to be independent of pH or concentration of the electrolyte solution, while the sharpness of the peak (P_I) increases with a lower pH (or higher anion concentration), especially for HSO_4^- and ClO_4^-. For the fluoride-containing electrolyte (Figure 2d), the situation for the P_I peaks is admittedly less clear, although there is a clear fluoride adsorption peak in the positive-going scan.

The potential for the phase transition of bi(sulfate) (Figure 2a) and methanesulfonate (Figure 2c), respectively, increases with pH at a rate of ca. 100 mV/pH, which indicates that it cannot correspond to a proton-coupled electron transfer (as that would shift 0 mV/pH). In the negative-going scan, the P_I peak potential (at 0.24, 0.29, 0.27, and 0.25 V_{RHE} for HSO_4^-, ClO_4^-, $CH_3SO_3H^-$, and F^-) is observed to be rather independent of pH or concentration of the electrolyte solution, while the sharpness of the peak (P_I) decreases with a lower anion concentration (also see Figure 3). In our model to be

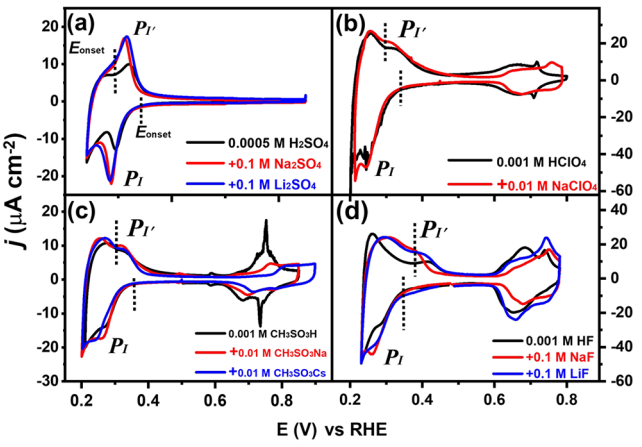

Figure 3. Cyclic voltammograms of Pd(111) in (a) 0.0005 M H_2SO_4, (b) 0.001 M $HClO_4$, (c) 0.001 M CH_3SO_3H, and (d) 0.001 M HF (pH 3) solutions without and with 0.01 and 0.1 M LiX, NaX, and CsX, where X is the corresponding anion. Scan rate: 20 mV s^{-1}.

discussed below, the anion adsorption/desorption process itself is fast, and the slow kinetics is due to the formation of subsurface hydrogen. A subsurface hydrogen phase exists during the positive-going scan as a result of the prior negative-going scan, while during the subsequent negative-going scan, there is far less subsurface hydrogen (depending on the employed scan rate and the potential range of the CV) and hence the corresponding reduction peak typically corresponds

https://doi.org/10.1021/jacsau.3c00343
JACS Au 2023, 3, 2780−2789

to fast anion desorption. As we discuss in the following part, the anion adsorption/desorption process itself is fast, and the slow kinetics is due to the subsurface hydrogen phase. A Pd subsurface hydrogen surface from hydrogen adsorption during a negative-going scan shows a weaker effect on anion adlayers than that of a Pd-hydride surface formed during a positive-going scan. The $P_{II'}/P_{II}$ peaks in the potential region of 0.60 < E < 0.95 V_{RHE} shift to a higher potential in the presence of a higher concentration of ClO_4^-, $CH_3SO_3H^-$, and F^-, suggesting a 'mixed anion−OH_{ads} feature' instead of a sole "OH_{ads} feature". The formation of OH_{ads} (eq 5) is very sensitive to the coadsorbing anion, presumably reflecting different anion adsorption modes and strengths. Figure 2 shows the $P_{II'}/P_{II}$ peaks shift to a more positive potential by decreasing electrolyte pH from 3 to 1 (and/or increasing anion concentration by ca. 1 and 2 orders of magnitude). Figure 3 further shows the formation of OH_{ads} is indeed inhibited, i.e., shifts to a more positive potential and with lower charge, when increasing the anion concentration at a constant pH. A consistent explanation for this effect of anion, which is identical to the results from $Pd_{ML}Pt(111)$ electrode,[28] is that the $P_{II'}/P_{II}$ peak involves the specific adsorption of anion or the strong interaction of the anion with the OH_{ads} layer. As mentioned, the combination of a broad and sharp peak, as in 0.001 M $HClO_4$ (Figure 2b, orange line), is very typical for a disorder−order transition in the OH adlayer. Also, this phase transition seems to be diminished due to a stronger interference from a more favorable ClO_4^- adsorption in 0.01 and 0.1 M $HClO_4$ (Figure 2b, pink and brown line).

Figure 3a shows cyclic voltammograms for the Pd(111) electrode in 0.0005 M H_2SO_4 (pH = 3) electrolytes with and without the addition of 0.1 M Li_2SO_4 and Na_2SO_4. In the presence of 0.1 M Li_2SO_4 and Na_2SO_4, the $P_{I'}/P_I$ peak current density increases considerably and the peak potential shifts to more negative potential, although the onset potential remains the same as that in 0.0005 M H_2SO_4 (pH = 3). There is no cation identity effect, i.e., Li^+ vs Na^+, on the adsorption/desorption process ($P_{I'}/P_I$). Figure S4 shows that the increase of current density of the $P_{I'}/P_I$ peak for the cyclic voltammogram of Pd(111) electrode recorded in 0.0005 M H_2SO_4 (pH = 3) is smaller with a lower concentration of cation (and anion), i.e., 0.01 M Li_2SO_4 and Na_2SO_4. Figure 3b−d shows cyclic voltammograms for the Pd(111) electrode in 0.001 M $HClO_4$, 0.001 M CH_3SO_3H, and 0.001 M HF (pH = 3) electrolytes with and without the addition of 0.1 M LiX and NaX. An important observation in Figure 3 is that the oxidation peak between 0.2 and 0.4 V is not sensitive to the nature of the cation in the sulfate and fluoride electrolytes. These results would imply that the process ($P_{I'}/P_I$) is devoid of hydroxyl adsorption, as the cation would be expected to cause a peak potential shift to a more positive value due to its destabilization of the "hydroxyl-cation" adlayer, as we observed previously for the step-related "hydrogen" peaks on stepped Pt electrodes[49,50] and $Pd_{ML}Pt(111)$ electrodes.[28] At the same pH and, hence, at the same interfacial electric field strength at a given potential (RHE), a higher anion concentration leads to stronger adsorption ($P_{I'}$) and the observation of a peak potential shift to a more negative value (Figures 3 and S4). Therefore, it is safe to conclude that the $P_{I'}/P_I$ peak on the Pd(111) electrode only involves anion adsorption/desorption immediately following/preceding the H_{upd} region.

The "OH_{ads} feature" (eq 5) in the potential region of 0.60 < E <0.95 V_{RHE} shifts to a higher potential in the presence of 0.1 M $NaClO_4$, CH_3SO_3Na, and NaF (Figure 3b−d), which is caused by the suppression of this feature by an increased anion adsorption and consistent with the results from Figure 2.

Moreover, the voltammetric profiles of the Pd(111) electrode in Figure 3b−d reveal that there is a discernible effect of the cation identity on the "OH_{ads} feature": for lithium, an earlier onset potential and a larger current are observed than for sodium and cesium. Following previous studies on the Pt(111) electrode, this could be interpreted as more strongly attractive (or less repulsive) interactions between OH_{ads} in the presence of Li^+, thereby stabilizing the OH adlayer[51] and decreasing the suppressive effect caused by the anion adsorption.

A peculiar characteristic of the anion desorption (P_I) and adsorption ($P_{I'}$) peaks is their irreversibility (as shown in Figures 1−3), indicating a kinetically limited process. Such a slow anion adsorption process is unexpected as it is not typically observed on Pt and $Pd_{ML}Pt(111)$ single-crystal electrodes (see Figure S1 in the Supporting Information). For irreversible processes, the peak potential (E_p) is expected to shift with the scan rate (ν) following $|E_p - E^\circ| \propto \ln(\frac{\nu}{k})$, where k is the rate constant and E° is the equilibrium potential for the reaction.[52,53] As indicated, the peak potential for the oxidation reaction ($E_{PI'}$) shifts to more positive values and the peak potential for the reduction reaction (E_{PI}) shifts to more negative values with increasing scan rates. Figure 4a shows that the irreversible behavior of the peak corresponding to the H/anion replacement reaction, i.e., 0.237 V_{RHE} for the negative-going scan and 0.300 V_{RHE} for the positive-going scan recorded at 100 mV s^{-1} in 0.05 M H_2SO_4 (pH = 1.3), disappears at a sufficiently low scan rate of 1 mV s^{-1} ($E_{PI} = E_{PI'} = 0.274$ V_{RHE}). In addition, Figure S5 shows that the peak attributed to the phase transition in the (bi)sulfate and methanesulfonate adlayer is reversible and independent of the scan rate. Figure 4b−d shows that for more weakly adsorbed anions, namely, perchlorate, methanesulfonate, and fluoride, the irreversibility of the peak corresponding to the H/anion replacement reaction also decreases when lower scan rates are employed. For such an irreversible surface-confined electron transfer reaction, the dependence of the anodic and cathodic peak potentials ($E_{PI'}$ and E_{PI}) on the logarithm of the scan rate (log ν) resembles a classical "trumpet plot".[53] The peak ($P_{I'}/P_I$) associated process is related to a heterogeneous ad/desorption step instead of a diffusion process and the following general equations express the anodic and the cathodic peak potential:[52]

$$E_{PI'} = E^\circ - \frac{RT}{\alpha nF}\ln\left(\frac{\alpha nF\nu}{RTk^\circ}\right) \quad (6)$$

$$E_{PI} = E^\circ + \frac{RT}{(1-\alpha)nF}\ln\left(\frac{(1-\alpha)nF\nu}{RTk^\circ}\right) \quad (7)$$

where k° is the rate constant at E°, the formal potential of the surface-confined redox couple, α is the (effective) transfer coefficient, E is the applied potential, ν is the applied scan rate, R is the universal gas constant (8.314 J K^{-1} mol^{-1}), T is the temperature, and F is Faraday's constant (96485 C mol^{-1}). When plotting E_p vs log ν, the slopes of these plots in principle correspond to Tafel slopes, though it is difficult to assign linear regions. No clear values or trends can be extracted from these slopes.

To explore the origin of the striking sluggish kinetics and mechanism of anion adsorption on the Pd(111) electrode, we

https://doi.org/10.1021/jacsau.3c00343
JACS Au 2023, 3, 2780−2789

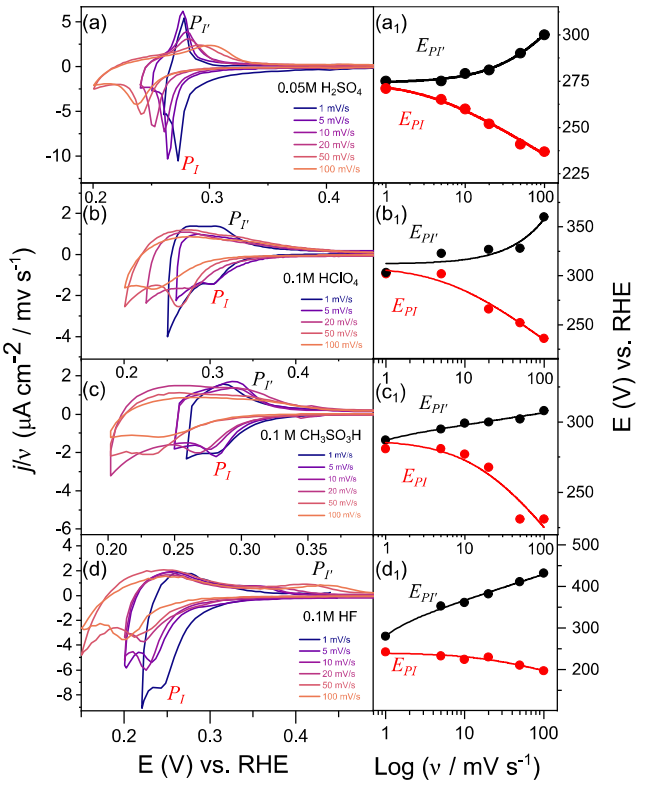

Figure 4. Cyclic voltammograms of Pd(111) electrode in (a) 0.05 M H_2SO_4, (b) 0.1 M $HClO_4$, (c) 0.1 M CH_3SO_3H, and (d) 0.1 M HF solutions recorded at various scan rates (and plotted as current density divided by scan rate). "Trumpet plots" displaying the anion adsorption ($P_{I'}$) and desorption (P_I) peak potentials as a function of the logarithm of scan rate in (a_1) 0.05 M H_2SO_4, (b_1) 0.1 M $HClO_4$, (c_1) 0.1 M CH_3SO_3H, and (d_1) 0.1 M HF solutions; the dots represent the experimental data points and the solid lines show the fit results.

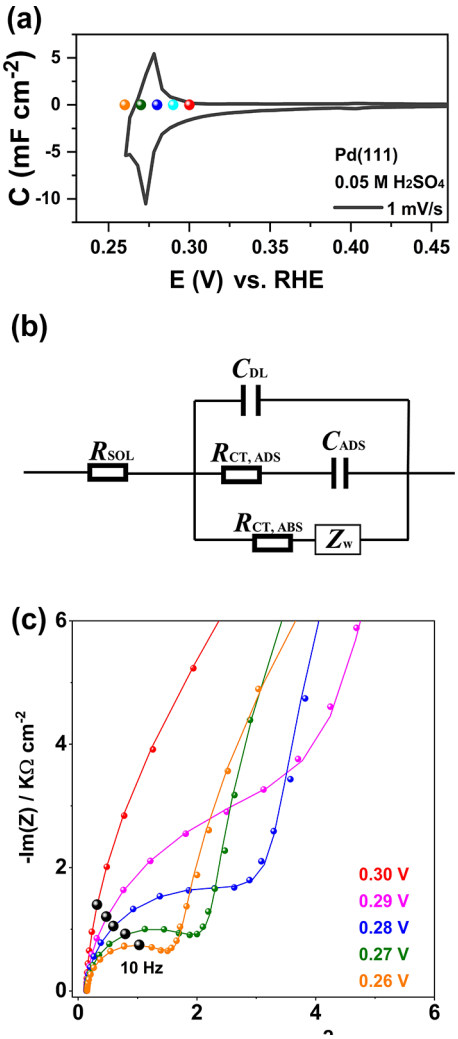

Figure 5. (a) Cyclic voltammogram of the Pd(111) electrode in 0.05 M H_2SO_4 recorded at 1 mV s^{-1} (plotted as capacitance, that is, the total current density divided by the scan rate). The different colors represent the potentials at which the data were collected. (b) The equivalent electric circuit (EEC) that is used to fit experimental impedance data, featuring the R_s term for solution resistance, the charge transfer resistance for the hydrogen and/or anion adsorption, $R_{ads,CT}$, in series with an adsorption capacitance, C_{ads}. In the presence of the direct hydrogen absorption, there is an additional parallel branch consisting of the absorption resistance, $R_{abs,CT}$, in series with a Warburg impedance, Z_W, corresponding to hydrogen diffusion into the bulk of Pd(111). (c) Typical Nyquist plots for Pd(111) in 0.05 M H_2SO_4. The dots represent the data points collected at anion and/or hydrogen ad/desorption region as indicated in Figure 5a, while the solid lines correspond to the fit obtained using the EEC. Data points at a frequency of 10 Hz are indicated with a black dot.

employed electrochemical impedance spectroscopy (EIS). The experimental impedance spectra were fitted using the equivalent electric circuit (EEC) presented in Figure 5b, which corresponds to a simple heterogeneous ad/desorption step, forming an adsorbed intermediate without diffusion limitation for the hydrogen and/or anion adsorption[54−56] in parallel with a typical diffusional process of hydrogen absorption/penetration into the Pd bulk.[57] Figures 5c and S6b show experimental and fitted spectra (Nyquist plot) of the Pd(111) electrode obtained in the potential regions of anion and/or hydrogen adsorption (as indicated in Figures 5a and S6a) in contact with 0.05 M H_2SO_4 and 0.1 M HF solutions, respectively. In Figures 5c and S6b, a high-frequency semicircle followed by a capacitive part at lower frequencies is observed. With a decrease of the applied potential, in the anion and/or hydrogen adsorption region, the low-frequency impedance line becomes more tilted (Figures 5c and S6b), which is attributed to the hydrogen absorption leading to the Warburg impedance as typical for a semi-infinite diffusional process.

Figure 6 shows the dependence of the parameters R_S, $R_{ads,CT}$, $R_{abs,CT}$, C_{DL}, and C_{ads} on the electrode potential in 0.05 M H_2SO_4. Figures 6 and S7 show the solution resistance, R_S, is independent of the applied potential and is 130 and 185 Ω in 0.05 M H_2SO_4 and 0.1 HF, respectively The double layer capacitance, C_{DL}, varies little around 10 ± 2 and 30 ± 5 μF cm^{-2} for 0.05 M H_2SO_4 and 0.1 M HF solutions, respectively, in rather good agreement with recent studies on double layer capacitances of Pd(111) electrodes.[39] Consistent with the blank voltammogram result in Figures 5a and S6a, Figures 6 and S7 show the adsorption capacitance, C_{ads}, increases to 189 μF cm^{-2} in the (bi)sulfate/hydrogen adsorption region (0.27 V_{RHE}) and 215 μF cm^{-2} in the fluoride/hydrogen adsorption region (0.33 V_{RHE}), respectively. Figure 6 shows a broad relatively potential independent plateau on the curve of the hydrogen absorption resistance, $R_{abs,CT}$, and increase of sulfate anion adsorption charge transfer resistance, $R_{ads,CT}$, with potential, respectively, in the potential region of (bi)sulfate

https://doi.org/10.1021/jacsau.3c00343
JACS Au 2023, 3, 2780−2789

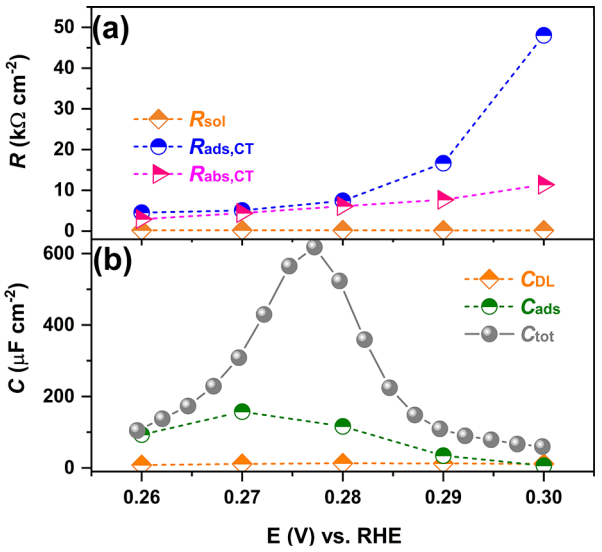

Figure 6. Fitted EIS data as a function of the applied potential in 0.05 M H_2SO_4. C_{tot} is calculated from the CV current.

adsorption (0.26 < E <0.30 V_{RHE}). Figure S7 also shows the hydrogen absorption resistance, $R_{abs,CT}$, also varies little in the potential region of fluoride adsorption region (0.24 < E <0.35 V_{RHE}). The hydrogen absorption process happens more easily, i.e., has a smaller charge transfer resistance ($R_{abs,CT}$) than that of anion adsorption ($R_{ads,CT}$) (Figures 6 and S7). To convince ourselves that hydrogen absorption is really coupled to diffusion, we have replaced the Warburg impedance in Figures 5b and S6b with a constant phase element (CPE), Z_{CPE}, as shown in Figures S8b and S9b for 0.05 M H_2SO_4 and 0.1 HF, respectively. We find that the optimal fit value for the corresponding CPE exponent (n) is ∼0.6 (Figures S8c and S9c), close to the value of 0.5 corresponding to a diffusion process.

Considering that the hydrogen absorption occurs at E < 0.40 V_{RHE},[57] the slowness, as well as the potential dependence, of the anion adsorption process, as expressed in $R_{ads,CT}$, could be related to the existence of hydrogen atoms in subsurface layers and the formation of PdH_x (palladium hydride) surface. This is corroborated by the observation (Figure S1) that this irreversibility is absent on the $Pd_{ML}Pt(111)$ electrode where such subsurface hydrogen formation does not occur. Since this process of subsurface hydrogen is coupled to the diffusion of hydride into the bulk, it is inherently slow and irreversible. Using impedance measurements of hydrogen diffusion into Pd, Gabrielli et al.[58] reported diffusion coefficient values of ca. 3−5 × 10^{-7} cm^2 s^{-1} for palladium foils between 0.11 and 0.20 V. Han et al.[59] reported a typical hydrogen permeation time scale of ca. 200 s for palladium foils at 0.20 V for a steady-state permeation current density of ca. 5 μA cm^{-2}. We posit here that this process is coupled with the irreversibility of the $P_I/P_{I'}$ redox couple. It has been found that hydride formation in palladium causes the lattice constant of palladium hydride to be higher than that characteristic of palladium[60,61] (by ∼3.5% compared to Pd[62]), as well as drastic changes of the surface potential (leading to an effective lowering of the work function). These changes have been ascribed to a corrugation as a result of stress creation and its relaxation within the PdH_x leads to a "roughening" of palladium, which is quite reversible.[60] The work function changes of the PdH_x surface have been interpreted according to the well-known Smolu-chowski's model,[63] that is, the increase of surface roughness would lower the work function. The lower work function of PdH_x would significantly favor anion adsorption and all anions studied here (HSO_4^-, ClO_4^-, $CH_3SO_3^-$, and F^-) adsorb specifically at E < 0.40 V_{RHE}. An alternative explanation could be that the presence of subsurface hydrogen introduces strain and ligand effects that slow anion adsorption. Future computational work on anion adsorption on PdH_x surfaces should further clarify this issue.

Notably, a PdH_x system would also change parameters such as the binding energy and/or the equilibrium coverage of surface absorbates and ultimately influence the adsorption process. Density functional theory (DFT) calculations indicate that adsorbates, i.e., H, acetylene, vinyl, and ethylene, bind weaker to a Pd(111) surface with subsurface layer hydrogen than to the Pd(111) surface.[64−67] We expect that the slow diffusion of hydride formation is superimposed on the surface processes. Therefore, the anion adsorption itself is not slow but rather the hydride absorption process altering the anion adsorption energetics.

CONCLUSIONS

In summary, voltammetric profiles of Pd(111) in acidic electrolytes consisting of various anions (HSO_4^-, ClO_4^-, $CH_3SO_3H^-$, and F^-) were reported and analyzed. In the so-called H_{upd} region, a couple of sharp peaks ($P_I/P_{I'}$) have been related to a surface replacement reaction of adsorbed hydrogen by anion electro-sorption, with the adsorption strength following the order of HSO_4 > ClO_4 > CH_3SO_3H > F. Strongly adsorbed anions also block/suppress the hydroxyl/oxide adsorption states at higher potentials in a corresponding manner. In particular, anion adsorption on Pd(111) is considerably stronger than on Pt(111) and even perchlorate and fluoride must be considered to be specifically adsorbed on Pd(111). Surprisingly, anion adsorption and desorption appear to be a kinetically limited process, which is in strong contrast to other Pt-group single-crystal electrodes. Detailed exploration to identify the nature of this unusual phenomenon with electrochemical impedance spectroscopy shows that anion adsorption/desorption is accompanied by desertion/insertion of hydride into the subsurface layers of the Pd(111) electrode surface, leading to the formation of Pd hydrides (PdH_x). The observed irreversibility is then explained by the lower adsorption energy of anions on a Pd-hydride surface, with the time dependence arising from the diffusion of hydride in and out of the Pd surface layers. This work thereby generates fundamentally new insights into the surface chemistry of well-defined Pd surfaces, which we hope will contribute to the development of this important electrocatalytic material.

EXPERIMENTAL DETAILS

Cyclic voltammetry measurements were carried out in standard electrochemical cells by using a three-electrode assembly at room temperature. Experiments were performed in a fluorinated ethylene propylene (PEP, Nalgene) electrochemical cell for hydrofluoric acid, and a glass cell was used for the other electrolytes. PEP cell was cleaned in freshly prepared piranha (3:1 v/v H_2SO_4 (96%, Suprapur) and H_2O_2 (30%, Merck Suprapur) over 2 h followed by at least five times repetitive rinsing and boiling with ultrapure water (Milli-Q, 18.2 MΩ cm). All glassware was cleaned in an acidic solution of potassium permanganate overnight, followed by rinsing with an acidic solution of hydrogen peroxide, repetitive rinsing, and boiling with ultrapure water.

https://doi.org/10.1021/jacsau.3c00343
JACS Au 2023, 3, 2780−2789

A palladium wire was used as counter electrode, and a reversible hydrogen electrode (RHE) was employed as the reference electrode, in a separate compartment filled with the same electrolyte, at the same pH as the electrolyte in the electrochemical cell. All potentials are reported versus the RHE. A Pd bead-type electrode (MaTecK) with a diameter of 4 mm and a Pd wire attached to its rear for better handling was used as the working electrode. Prior to each experiment, the Pd working electrode was annealed by inductive heating in an inert, all-quartz tube, which was filled with a stream of argon. Subsequently, the electrode was slowly cooled down to room temperature in an argon stream and the contact with the electrolyte was established under potential control (around 0.45 V_{RHE}), where no H absorption occurred. The electrochemical measurements were performed with the single-crystal electrode in the hanging meniscus configuration. The potential was controlled with a BioLogic VSP-300 potentiostat by using proprietary software. The current density shown in the manuscript represents the measured current normalized to the geometric area of the working electrode. Inductive heating was applied via a 2.4 kW Ambrell EASYheat model 0224 fitted with a Flowmax water cooling solution. The Ar stream (Air Products, 5.7) during cooling processes was digitally controlled by using a mass flow controller (SLA5850, Brooks). Electrochemical impedance spectroscopy (EIS) was conducted with a Biologic VSP-300 potentiostat. Nyquist plots were measured with frequencies ranging from 10 kHz to 0.1 Hz with an amplitude of 5 mV.

Electrolytes were made from ultrapure water (Milli-Q, 18.2 MΩ cm), high purity reagents $HClO_4$ (70%), H_2SO_4 (96%), CH_3SO_3H (>99.0%), HF (40%), Li_2SO_4 (99.99%), Na_2SO_4 (99.99%), $NaClO_4$ (99.99%), $LiClO_4$ (99.99%), CH_3SO_3Li (99.99%), CH_3SO_3Na (90%), LiF (99.995%), and NaF (99.99%) from Merck Suprapur. Before each experiment, the electrolytes were first purged with argon for at least 30 min to remove air from the solution.

■ ASSOCIATED CONTENT

Supporting Information

The Supporting Information is available free of charge at https://pubs.acs.org/doi/10.1021/jacsau.3c00343.

Additional cyclic voltammetry data, additional electrochemical impedance spectroscopy data (PDF)

■ AUTHOR INFORMATION

Corresponding Author

Marc T. M. Koper − *Leiden Institute of Chemistry, Leiden University, Leiden 2300 RA, The Netherlands;* orcid.org/0000-0001-6777-4594; Email: m.koper@chem.leidenuniv.nl

Authors

Xiaoting Chen − *School of Materials Science and Engineering, Beijing Institute of Technology, Beijing 100081, P.R. China; Leiden Institute of Chemistry, Leiden University, Leiden 2300 RA, The Netherlands*

Kasinath Ojha − *Leiden Institute of Chemistry, Leiden University, Leiden 2300 RA, The Netherlands;* orcid.org/0000-0002-3811-8579

Complete contact information is available at: https://pubs.acs.org/10.1021/jacsau.3c00343

Notes

The authors declare no competing financial interest.

■ ACKNOWLEDGMENTS

Xiaoting Chen acknowledges support from the China Scholarship Council (award number 201506220154).

■ REFERENCES

(1) Hanifah, M. F. R.; Jaafar, J.; Othman, M. H. D.; Yusof, N.; Rahman, M. A.; Salleh, W. N. W.; Ismail, A. F.; Aziz, F.; Rehman, G. U. One-step fabrication of a highly dispersed palladium nanoparticle-decorated reduced graphene oxide electrocatalyst for methanol electro-oxidation in acidic media. *J. Phys. Chem. Solids* **2021**, *148*, No. 109718.

(2) Chen, X.; Koper, M. T. Mass-transport-limited oxidation of formic acid on a PdMLPt (100) electrode in perchloric acid. *Electrochem. Commun.* **2017**, *82*, 155−158.

(3) Ding, J.; Liu, Z.; Liu, X.; Liu, B.; Liu, J.; Deng, Y.; Han, X.; Hu, W.; Zhong, C. Tunable periodically ordered mesoporosity in palladium membranes enables exceptional enhancement of intrinsic electrocatalytic activity for formic acid oxidation. *Angew. Chem., Int. Ed.* **2020**, *132* (13), 5130−5139.

(4) Liang, Z.; Villalba, M. A.; Marcandalli, G.; Ojha, K.; Shih, A. J.; Koper, M. T. Electrochemical Reduction of the Simplest Monosaccharides: Dihydroxyacetone and Glyceraldehyde. *ACS Catal.* **2020**, *10* (23), 13895−13903.

(5) Liang, Z.; Villalba, M. A.; Koper, M. T. Structure sensitivity of electrochemical adsorption and reduction of acetol on noble metal electrodes. *Electrochim. Acta* **2021**, *391*, No. 138911.

(6) Villalba, M. A.; Koper, M. T. Structure Sensitivity of Acetophenone Reduction on Palladium-Modified Platinum Single-Crystal Electrodes. *J. Phys. Chem. C* **2020**, *124* (47), 25884−25891.

(7) Huang, H.; Jia, H.; Liu, Z.; Gao, P.; Zhao, J.; Luo, Z.; Yang, J.; Zeng, J. Understanding of strain effects in the electrochemical reduction of CO2: using Pd nanostructures as an ideal platform. *Angew. Chem., Int. Ed.* **2017**, *129* (13), 3648−3652.

(8) Chatterjee, S.; Griego, C.; Hart, J. L.; Li, Y.; Taheri, M. L.; Keith, J.; Snyder, J. D. Free standing nanoporous palladium alloys as CO poisoning tolerant electrocatalysts for the electrochemical reduction of CO2 to formate. *ACS Catal.* **2019**, *9* (6), 5290−5301.

(9) Min, X.; Kanan, M. W. Pd-catalyzed electrohydrogenation of carbon dioxide to formate: high mass activity at low overpotential and identification of the deactivation pathway. *J. Am. Chem. Soc.* **2015**, *137* (14), 4701−4708.

(10) Humphrey, J. J.; Plana, D.; Celorrio, V.; Sadasivan, S.; Tooze, R. P.; Rodríguez, P.; Fermín, D. Electrochemical reduction of carbon dioxide at gold-palladium core−shell nanoparticles: product distribution versus shell thickness. *ChemCatChem* **2016**, *8* (5), 952−960.

(11) Shin, H.; Jung, S.; Bae, S.; Lee, W.; Kim, H. Nitrite reduction mechanism on a Pd surface. *Environ. Sci. Technol.* **2014**, *48* (21), 12768−12774.

(12) Lim, J.; Liu, C.-Y.; Park, J.; Liu, Y.-H.; Senftle, T. P.; Lee, S. W.; Hatzell, M. C. Structure Sensitivity of Pd Facets for Enhanced Electrochemical Nitrate Reduction to Ammonia. *ACS Catal.* **2021**, *11*, 7568−7577.

(13) Clavilier, J.; Faure, R.; Guinet, G.; Durand, R. Preparation of monocrystalline Pt microelectrodes and electrochemical study of the plane surfaces cut in the direction of the {111} and {110} planes. *J. Electroanal. Chem. Interfacial Electrochem.* **1980**, *107* (1), 205−209.

(14) Clavilier, J.; El Achi, K.; Rodes, A. In situ characterization of the Pt (S)-[n (111)/sx (111)] electrode surfaces using electrosorbed hydrogen for probing terrace an step sites. *J. Electroanal. Chem. Interfacial Electrochem.* **1989**, *272* (1−2), 253−261.

(15) Motoo, S.; Furuya, N. Hydrogen and oxygen adsorption on Ir (111), (100) and (110) planes. *J. Electroanal. Chem. Interfacial Electrochem.* **1984**, *167* (1−2), 309−315.

(16) Motoo, S.; Furuya, N. Effect of anions on hydrogen and oxygen adsorption on iridium single cyrstal surfaces. *J. Electroanal. Chem. Interfacial Electrochem.* **1984**, *181* (1−2), 301−305.

(17) Clavilier, J.; Wasberg, M.; Petit, M.; Klein, L. Detailed analysis of the voltammetry of Rh (111) in perchloric acid solution. *J. Electroanal. Chem. Interfacial Electrochem.* **1994**, *374* (1−2), 123−131.

(18) El-Aziz, A.; Kibler, L. New information about the electrochemical behaviour of Ru (0 0 0 1) in perchloric acid solutions. *Electrochem. Commun.* **2002**, *4* (11), 866−870.

(19) Hoster, H.; Behm, R. The effect of structurally well-defined Pt modification on the electrochemical and electrocatalytic properties of Ru (0001) electrodes. In *Fuel Cell Catalysis: A Surface Science Approach*; 2009; vol *1*, p 465.
(20) Alvarez, B.; Climent, V.; Rodes, A.; Feliu, J. Anion adsorption on Pd−Pt (111) electrodes in sulphuric acid solution. *J. Electroanal. Chem.* **2001**, *497* (1−2), 125−138.
(21) Gabrielli, C.; Grand, P.; Lasia, A.; Perrot, H. Investigation of hydrogen adsorption and absorption in palladium thin films: II. Cyclic voltammetry. *J. Electrochem. Soc.* **2004**, *151* (11), A1937.
(22) Sarac, B.; Sarac, A. S.; Eckert, J. Pd-based Metallic Glasses as Promising Materials for Hydrogen Energy Applications. *J. Electrochem. Soc.* **2023**, *170*, No. 014503.
(23) Mueller, W. M.; Blackledge, J. P.; Libowitz, G. G. *Metal hydrides*; Elsevier, 2013.
(24) Hu, C. C.; Wen, T. C. Effects of pH and Anion on Hydrogen Sorption/Desorption at/within Oxide-Derived Pd Electrodes. *J. Electrochem. Soc.* **1995**, *142* (5), 1376.
(25) Monteiro, M. C.; Goyal, A.; Moerland, P.; Koper, M. T. Understanding cation trends for hydrogen evolution on platinum and gold electrodes in alkaline media. *ACS Catal.* **2021**, *11* (23), 14328−14335.
(26) Llorca, M.; Feliu, J.; Aldaz, A. Clavilier, Electrochemical structure-sensitive behaviour of irreversibly adsorbed palladium on Pt (100), Pt (111) and Pt (110) in an acidic medium. *J. ElectroChem. Soc.* **1993**, *351* (1−2), 299−319.
(27) Alvarez, B.; Climent, V.; Rodes, A.; Feliu, J. M. Anion adsorption on Pd−Pt (111) electrodes in sulphuric acid solution. *J. Electrochem. Soc.* **2001**, *497* (1−2), 125−138.
(28) Chen, X.; Granda-Marulanda, L. P.; McCrum, I. T.; Koper, M. T. Adsorption processes on a Pd monolayer-modified Pt (111) electrode. *Chem. Sci.* **2020**, *11* (6), 1703−1713.
(29) Hara, M.; Linke, U.; Wandlowski, T. Preparation and electrochemical characterization of palladium single crystal electrodes in 0.1M H2SO4 and HClO4: Part I. Low-index phases. *Electrochim. Acta* **2007**, *52* (18), 5733−5748.
(30) Cuesta, A.; Kibler, L. A.; Kolb, D. M. A method to prepare single crystal electrodes of reactive metals: application to Pd (hkl). *J. Electroanal. Chem.* **1999**, *466* (2), 165−168.
(31) Hoshi, N.; Kuroda, M.; Koga, O.; Hori, Y. Infrared reflection absorption spectroscopy of the sulfuric acid anion on low and high index planes of palladium. *J. Phys. Chem. B* **2002**, *106* (35), 9107−9113.
(32) Hoshi, N.; Kuroda, M.; Ogawa, T.; Koga, O.; Hori, Y. Infrared reflection absorption spectroscopy of the sulfuric acid anion adsorbed on Pd (S)−[n (111)×(111)] electrodes. *Langmuir* **2004**, *20* (12), 5066−5070.
(33) Hoshi, N.; Koga, O.; Hori, Y.; Ogawa, T. Infrared reflection absorption spectroscopy of carbon monoxide adsorbed on Pd (S)-[n (1 1 1)×(1 1 1)] and Pd (S)-[n (1 0 0)×(1 1 1)] electrodes. *J. Electroanal. Chem.* **2006**, *587* (1), 79−85.
(34) Hoshi, N.; Kuroda, M.; Hori, Y. J. Voltammograms of stepped and kinked stepped surfaces of palladium: Pd (S)-[n (111)×(100)] and Pd (S)-[n (100)×(110)]. *J. Electroanal. Chem.* **2002**, *521* (1−2), 155−160.
(35) Hoshi, N.; Nakamura, M.; Maki, N.; Yamaguchi, S.; Kitajima, A. Structural effects on voltammograms of the low index planes of palladium and Pd (S)-[n (1 0 0)×(1 1 1)] surfaces in alkaline solution. *J. Electroanal. Chem.* **2008**, *624* (1−2), 134−138.
(36) Kiguchi, F.; Nakamura, M.; Hoshi, N. Structural effects on voltammograms of the high index planes of Pd in alkaline solution. *J. Electroanal. Chem.* **2021**, *880*, No. 114925.
(37) Hoshi, N.; Kagaya, K.; Hori, Y. Voltammograms of the single-crystal electrodes of palladium in aqueous sulfuric acid electrolyte: Pd (S)-[n (111)×(111)] and Pd (S)-[n (100)×(111)]. *J. Electroanal. Chem.* **2000**, *485* (1), 55−60.
(38) Koper, M. T. Blank voltammetry of hexagonal surfaces of Pt-group metal electrodes: comparison to density functional theory calculations and ultra-high vacuum experiments on water dissociation. *Electrochim. Acta* **2011**, *56* (28), 10645−10651.
(39) Gubanova, E.; Schmidt, T. O.; Watzele, S.; Alexandrov, V.; Bandarenka, A. S. Structure-Dependent Electrical Double-Layer Capacitances of the Basal Plane Pd (hkl) Electrodes in HClO4. *J. Phys. Chem. C* **2022**, *126* (27), 11414−11420.
(40) Naito, K.; Nakamura, M.; Sakata, O.; Hoshi, N. Surface X-ray scattering of Pd (111) and Pd (100) electrodes during the oxygen reduction reaction. *Electrochem.* **2011**, *79* (4), 256−260.
(41) Wan, L.-J.; Suzuki, T.; Sashikata, K.; Okada, J.; Inukai, J.; Itaya, K. In situ scanning tunneling microscopy of adsorbed sulfate on well-defined Pd (111) in sulfuric acid solution. *J. Electroanal. Chem.* **2000**, *484* (2), 189−193.
(42) Wei, Z.; Zhang, M. K.; Zhu, B. Q.; Xu, M. L.; Lei, J.; Tang, H.; Cai, J.; Chen, Y.-X. Effect of pH on Sulfate Adsorption on the Pd (111) Electrode. *J. Phys. Chem. C* **2022**, *126*, 3891−3902.
(43) El-Aziz, A.; Kibler, L. Influence of steps on the electrochemical oxidation of CO adlayers on Pd (111) and on Pd films electro-deposited onto Au (111). *J. Electroanal. Chem.* **2002**, *534* (2), 107−114.
(44) Kim, Y.-G.; Soriaga, J. B.; Vigh, G.; Soriaga, M. P. Atom-resolved EC-STM studies of anion adsorption at well-defined surfaces: Pd (111) in sulfuric acid solution. *J. Colloid Interface Sci.* **2000**, *227* (2), 505−509.
(45) Nakamura, M.; Sakurai, Y.; Ito, M. Sulfate and CO surface complexes formation with upd copper on Pd (111) and Pt (111) electrode surfaces: abnormal vibrational frequency shifts of CO and sulfate during upd processes. *J. Electroanal. Chem.* **2004**, *563* (1), 63−69.
(46) Garcia-Araez, N.; Climent, V.; Rodriguez, P.; Feliu, J. M. Elucidation of the chemical nature of adsorbed species for Pt (111) in H2SO4 solutions by thermodynamic analysis. *Langmuir* **2010**, *26* (14), 12408−12417.
(47) Koper, M. T.; Lukkien, J. Modeling the butterfly: influence of lateral interactions and adsorption geometry on the voltammetry at (111) and (100) electrodes. *Surf. Sci.* **2002**, *498* (1−2), 105−115.
(48) Frumkin, A.; Petrii, O. Potentials of zero total and zero free charge of platinum group metals. *Electrochim. Acta* **1975**, *20* (5), 347−359.
(49) Chen, X.; McCrum, I. T.; Schwarz, K. A.; Janik, M. J.; Koper, M. T. Co-adsorption of cations as the cause of the apparent pH dependence of hydrogen adsorption on a stepped platinum single-crystal electrode. *Angew. Chem., Int. Ed.* **2017**, *56* (47), 15025−15029.
(50) McCrum, I. T.; Chen, X.; Schwarz, K. A.; Janik, M. J.; Koper, M. T. Effect of step density and orientation on the apparent pH dependence of hydrogen and hydroxide adsorption on stepped platinum surfaces. *J. Phys. Chem. C* **2018**, *122* (29), 16756−16764.
(51) Stoffelsma, C.; Rodriguez, P.; Garcia, G.; Garcia-Araez, N.; Strmcnik, D.; Markovic, N. M.; Koper, M. T. Promotion of the oxidation of carbon monoxide at stepped platinum single-crystal electrodes in alkaline media by lithium and beryllium cations. *J. Am. Chem. Soc.* **2010**, *132* (45), 16127−16133.
(52) Bard, A. J.; Faulkner, L. R.; White, H. S. *Electrochemical methods: fundamentals and applications*; John Wiley & Sons, 2022.
(53) Laviron, E. General expression of the linear potential sweep voltammogram in the case of diffusionless electrochemical systems. *J. Electroanal. Chem. Interfacial Electrochem.* **1979**, *101* (1), 19−28.
(54) Lasia, A. Applications of electrochemical impedance spectroscopy to hydrogen adsorption, evolution and absorption into metals. In *Modern aspects of electrochemistry*; Springer, 2002; pp 1−49.
(55) Schouten, K.; Van Der Niet, M.; Koper, M. Impedance spectroscopy of H and OH adsorption on stepped single-crystal platinum electrodes in alkaline and acidic media. *Phys. Chem. Chem. Phys.* **2010**, *12* (46), 15217−15224.
(56) Morin, S.; Dumont, H.; Conway, B. Evaluation of the effect of two-dimensional geometry of Pt single-crystal faces on the kinetics of upd of H using impedance spectroscopy. *J. Electroanal. Chem.* **1996**, *412* (1−2), 39−52.

https://doi.org/10.1021/jacsau.3c00343
JACS Au 2023, 3, 2780−2789

(57) Duncan, H.; Lasia, A. Mechanism of hydrogen adsorption/absorption at thin Pd layers on Au(111). *Electrochim. Acta* **2007**, *52* (21), 6195−6205.
(58) Gabrielli, C.; Grand, P.; Lasia, A.; Perrot, H. Investigation of hydrogen adsorption and absorption in palladium thin films: III: Impedance spectroscopy. *J. Electrochem. Soc.* **2004**, *151* (11), A1943.
(59) Han, J. N.; Pyun, S.; Yang, T. H. Roles of thiourea as an inhibitor in hydrogen absorption into palladium electrode. *J. Electrochem. Soc.* **1997**, *144* (12), 4266.
(60) Duś, R.; Nowakowski, R.; Nowicka, E. Chemical and structural components of work function changes in the process of palladium hydride formation within thin Pd film. *J. Alloys Compd.* **2005**, *404*, 284−287.
(61) Mwanda, J. A.; Cuesta, A. Reduction of Pd2+ pre-adsorbed on cyanide-modified Pt (111) electrodes: adlayer metallization vs. metal-on-metal deposition. *Electrochim. Acta* **2018**, *292*, 419−424.
(62) Nowakowski, R.; Duś, R. Atomic force microscopy studies of thin Pd film response to palladium hydride formation and its reaction with oxygen. *Langmuir* **2003**, *19* (17), 6750−6758.
(63) Smoluchowski, R. Anisotropy of the electronic work function of metals. *Phys. Rev.* **1941**, *60* (9), 661.
(64) Johansson, M.; Skulason, E.; Nielsen, G.; Murphy, S.; Nielsen, R. M.; Chorkendorff, I. Hydrogen adsorption on palladium and palladium hydride at 1 bar. *Surf. Sci.* **2010**, *604* (7−8), 718−729.
(65) Sheth, P. A.; Neurock, M.; Smith, C. M. A first-principles analysis of acetylene hydrogenation over Pd (111). *J. Phys. Chem. B* **2003**, *107* (9), 2009−2017.
(66) Studt, F.; Abild-Pedersen, F.; Bligaard, T.; Sørensen, R. Z.; Christensen, C. H.; Nørskov, J. K. On the role of surface modifications of palladium catalysts in the selective hydrogenation of acetylene. *Angew. Chem., Int. Ed.* **2008**, *120* (48), 9439−9442.
(67) Wilde, M.; Fukutani, K.; Ludwig, W.; Brandt, B.; Fischer, J. H.; Schauermann, S.; Freund, H. J. Influence of carbon deposition on the hydrogen distribution in Pd nanoparticles and their reactivity in olefin hydrogenation. *Angew. Chem., Int. Ed.* **2008**, *47* (48), 9289−9293.

https://doi.org/10.1021/jacsau.3c00343
JACS Au 2023, 3, 2780−2789